

Transport reversals at Taiwan Strait during October and November 1999

D. S. Ko, R. H. Preller, and G. A. Jacobs

Naval Research Laboratory, Stennis Space Center, Mississippi, USA

T. Y. Tang and S. F. Lin

Institute of Oceanography, National Taiwan University, Taipei, Taiwan

Received 25 February 2003; revised 10 July 2003; accepted 12 September 2003; published 28 November 2003.

[1] The observed transport reversals at Taiwan Strait during October and November 1999 are examined by analytic solutions, a numerical ocean model, and the prediction from a real-time, North Pacific Ocean, data-assimilating model. Wind stress explains a majority of the transport reversals. The reversals are forced by a combination of the local wind and the remote wind in the Yellow and East China Seas. The connection between the Yellow and East China Seas wind stress and transport reversals at Taiwan Strait is provided by coastally trapped waves. The waves are generated by the northerly winter wind bursts in the Yellow Sea and are enhanced in the East China Sea by alongshore northerly wind. *INDEX TERMS*: 3339 Meteorology and Atmospheric Dynamics: Ocean/atmosphere interactions (0312, 4504); 4203 Oceanography: General: Analytical modeling; 4219 Oceanography: General: Continental shelf processes; 4255 Oceanography: General: Numerical modeling; *KEYWORDS*: ocean/atmosphere interactions, transport variation at strait, coastally trapped wave, numerical/analytical modeling, ocean prediction, continental shelf processes

Citation: Ko, D. S., R. H. Preller, G. A. Jacobs, T. Y. Tang, and S. F. Lin, Transport reversals at Taiwan Strait during October and November 1999, *J. Geophys. Res.*, 108(C11), 3370, doi:10.1029/2003JC001836, 2003.

1. Introduction

[2] The transport through the Taiwan Strait is generally northward from the South China Sea to the East China Sea even during the winter when the northerly monsoon prevails [Chuang, 1985, 1986]. Consequently, the sea level is higher along the Taiwan coast and decreases toward Chinese coast. From September to December 1999, transport through the Taiwan Strait was measured with four bottom-mounted acoustic Doppler current profilers (Figure 1). The time series shows strong transport reversals with roughly a biweekly period (Figure 2).

[3] Chern [1982] shows that in the winter the current at Taiwan Strait strongly responds to the wind. The atmospheric frontal systems pass through the east Asian seas from northwest to southeast with roughly a biweekly period during the winter. Strong wind bursts often accompany these frontal passages [Jacobs *et al.*, 1998b; Hsueh, 1988; Hu, 1944]. A strong northerly wind may reverse the sea surface slope across the Taiwan Strait and induce a geostrophic transport reversal.

[4] Within the Yellow Sea, the strong northerly winter-time wind bursts often excite coastally trapped waves. Hsueh [1988] and Hsueh and Pang [1989] connect winter current variations observed near the Korean coast to coastally trapped long waves in the Yellow Sea excited by the wind bursts. On the basis of the analyses of TOPEX/

Poseidon altimeter sea surface height (SSH) observations, Navy Operational Global Atmospheric Prediction System (NOGAPS)[Rosmond, 1992] wind stress fields, and ocean model simulations, Jacobs *et al.* [1998a, 1998b] show that the winter wind bursts excite a strong response by the sea surface heights in the Bohai Bay and Yellow Sea. The SSH changes produce the coastally trapped waves that propagate southward along the Chinese coast. The coastally trapped waves that enter the Taiwan Strait can reverse the sea surface slope across the strait and induce transport reversals.

[5] The objective of this study is to investigate the factors responsible for the transport reversals at Taiwan Strait by applying analytic solutions, a numerical ocean model, and the prediction from a real-time North Pacific Ocean data-assimilating model. Brief descriptions of the observations, the numerical ocean model, and the real-time prediction used for this study are given in section 2. The effect of the local wind on the transport variation is examined in section 3. The effect of remotely forced coastally trapped waves on the transport variation is examined in section 4. A conclusion is given in section 5.

2. Observations, Real-Time Prediction, and Numerical Model

2.1. Observations

[6] Current direction and speed were measured with acoustic Doppler current profilers (ADCP) mounted on the bottom at four locations across the Taiwan Strait at 25°N (Figure 1). The measured depth nearest to the sea

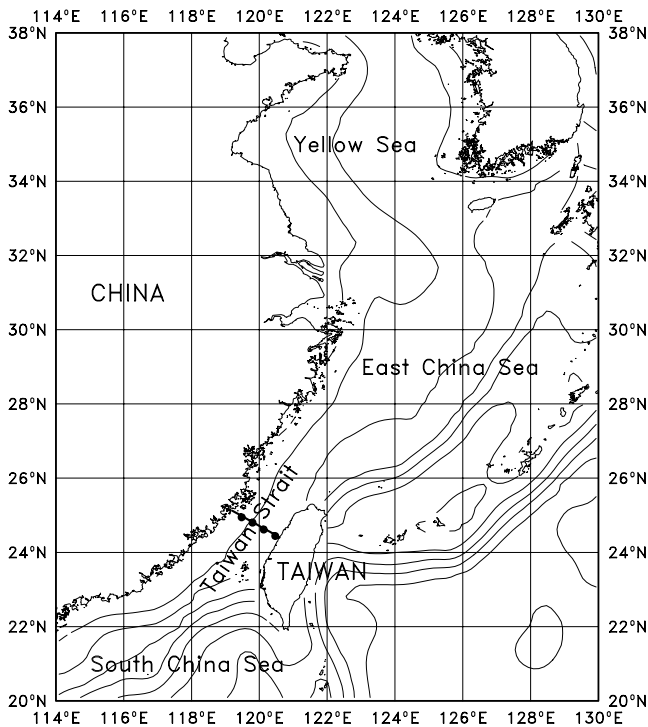


Figure 1. From September to December 1999, transport through Taiwan Strait was measured with bottom-mounted ADCP at four locations indicated by dots.

surface is 5 m, except for the station near the Chinese coast which is 13 m. The nearest bottom depth that can be measured is 3–4 m above the bottom. The water depths at the four stations are 44 m, 59 m, 65 m, and 53 m from west to east. The vertical resolution is 2 m. The measurement period was from September 28 to December 14, 1999. Tidal signals are removed by 48-hour low-pass filter. Hourly transport was computed from alongshore currents

after tide removal. Two months of transport data, in October and November, are used in the study.

2.2. Real-Time Prediction

[7] The prediction from a real-time North Pacific Ocean data-assimilating model, the North Pacific Ocean Nowcast/Forecast System (NPACNFS), operated at the Naval Research Laboratory is used for the study. The North Pacific Ocean (NPAC) model applied in the NPACNFS is based on the Princeton Ocean Model (POM) [Blumberg and Mellor, 1987]. Modifications were made to accommodate data assimilation. The model domain covers the North Pacific Ocean, the Equatorial Pacific, and part of the Indian Ocean from 16°S to 60°N and 99°E to 77°W. The grid resolution is 40 km at the equator and decreases to 20 km at the northern boundary. Twenty-six sigma levels (0.000, -0.001, -0.003, -0.006, -0.010, -0.015, -0.020, -0.025, -0.030, -0.035, -0.045, -0.065, -0.105, -0.165, -0.245, -0.325, -0.405, -0.485, -0.565, -0.645, -0.725, -0.805, -0.885, -0.945, -0.985, -1.000) are used with denser levels at top to better resolve the upper-ocean variations. A seasonally varying outflow of 8 ± 2 Sv ($10^6 \text{ m}^3/\text{s}$) (6 Sv at winter and 10 Sv at summer) is specified along the western boundary at the Indian Ocean according to estimates of the Indonesia Through Flow. Outflow of 3 ± 2 Sv (5 Sv at winter and 1 Sv at summer) is specified along the northern boundary at the Bering Sea. An inflow along the southern boundary at the South Pacific is specified to balance the outflows.

[8] Satellite altimeter data and Multi-Channel Sea Surface Temperature (MCSST) are used for data assimilation. A statistical model, the Modular Ocean Data Assimilation System (MODAS) [Carnes *et al.*, 1996] is applied to produce 3D ocean temperature/salinity analyses from satellite data. Every 24 hours, the model is restarted from its own fields at -48 hours. Once it is restarted, the model temperature/salinity are continuously modified toward the analyses using a vertical weighting function. The weighting reflects the relative confidence between the model and the analyses.

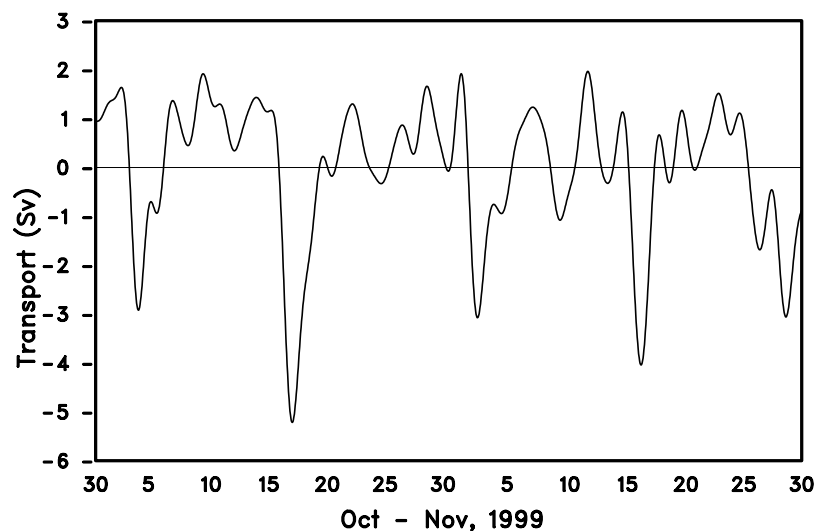


Figure 2. Measured hourly transport time series at October and November 1999, 48-hour low-pass filtered. It shows strong reversals of transport with roughly a biweekly period. The mean transport is 0.2 Sv.

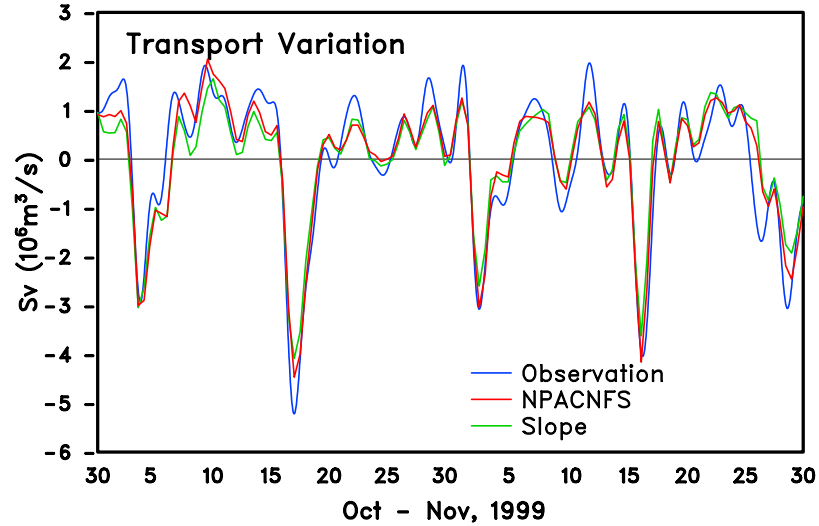


Figure 3. Transport variation time series from NPACNFS (red line) and from the geostrophic current estimated from NPACNFS mean sea surface slope (green line) compared to the observations (blue line).

[9] Surface forcing of wind stress, heat flux, solar radiation, and the sea level air pressure is derived from NOGAPS. The solar radiation is separated from the total heat flux. The rest of the heat flux is adjusted by the differences between the model sea surface temperature (SST) and the MCSSTs, and between the model SST and the seasonal climatology. The surface saline flux is estimated from the differences between model sea surface salinity (SSS) and the analysis, and between model SSS and the seasonal climatology. The 12-hourly NPACNFS predictions at 0000 UT and 1200 UT are used for this study.

[10] The transport variation at Taiwan Strait, calculated from NPACNFS vertical integrated velocity, compares very well with the ADCP observations (Figure 3). The favorable comparison suggests that the NPACNFS adequately represents the mechanisms controlling the transport variation at the strait.

[11] Applying the geostrophic balance, the transport variation is estimated from the NPACNFS sea surface height difference across the strait (sea surface slope). The estimated transport variation explains a major portion of the observed variation (Figure 3). This indicates that the dominant dynamics governing the transport variations through the Taiwan Strait in the winter is in geostrophic balance when the water is well mixed.

2.3. Numerical Model

[12] A smaller domain and simplified model was adapted from the NPAC ocean model for the study. The model domain is reduced to cover only the study area which includes the Yellow Sea, East China Sea, Taiwan Strait, and northern part of South China Sea. Near the Chinese coast and in the Taiwan Strait, the water depth is shallow and the water is well mixed during the winter. To isolate the dynamical issues, the model solves for only the hydrodynamic portion of the primitive equations. The vertical eddy diffusion is provided by the Mellor-Yamada 2.5-level closure model [Mellor and Yamada, 1982] as in POM, except the internal turbulent kinetic energy is produced by the vertical current shear alone. On the lateral open boundaries,

a gravity wave radiation boundary condition is prescribed. Wind stress is the only forcing applied to the model in this study.

3. Local Wind Effect

[13] An analytic solution relating the transport through a strait to the local alongshore wind stress may be derived from Ekman transport, continuity, and geostrophy. The relation between wind stress and transport in the open ocean has long been described by *Ekman* [1905]. For a wind in the y -direction, the transport may be defined by

$$S_x = (\tau_y/\rho)/f, \quad (1)$$

where τ_y is the wind stress, ρ is the water density, and f the Coriolis parameter. The unit volume transport, S_x , is directed 90° to the right of wind direction in the Northern Hemisphere.

[14] In an open ocean, Ekman transport may continue in the horizontal indefinitely. However, when applying it to a strait, the limitation of coastal boundaries must produce a setup of water on one side and a set-down on the opposite side (Figure 4). Although it is not necessary, a constant depth is used to derive the analytic solution. The change of sea level or sea surface elevation (depression), η , can be obtained by satisfying the continuity equation. The instantaneous, stationary solution is

$$\eta = -(+) S_x / (L/2), \quad (2)$$

where L is the width of strait. The mean sea surface slope across the strait is $d\eta/dx = -2\eta/(L/2) = 8 S_x/L^2$.

[15] Applying the geostrophic balance, $fv = g d\eta/dx$, where g is the gravitational acceleration, the geostrophic current, v , can be derived from the sea surface slope. The transport through the strait, S_v , is obtained by integrating the current over the depth, H , and the width of the strait, $S_v = 8 (gH/f)S_x/L$. It can be directly related to the alongshore local wind stress from equation (1), the Ekman transport,

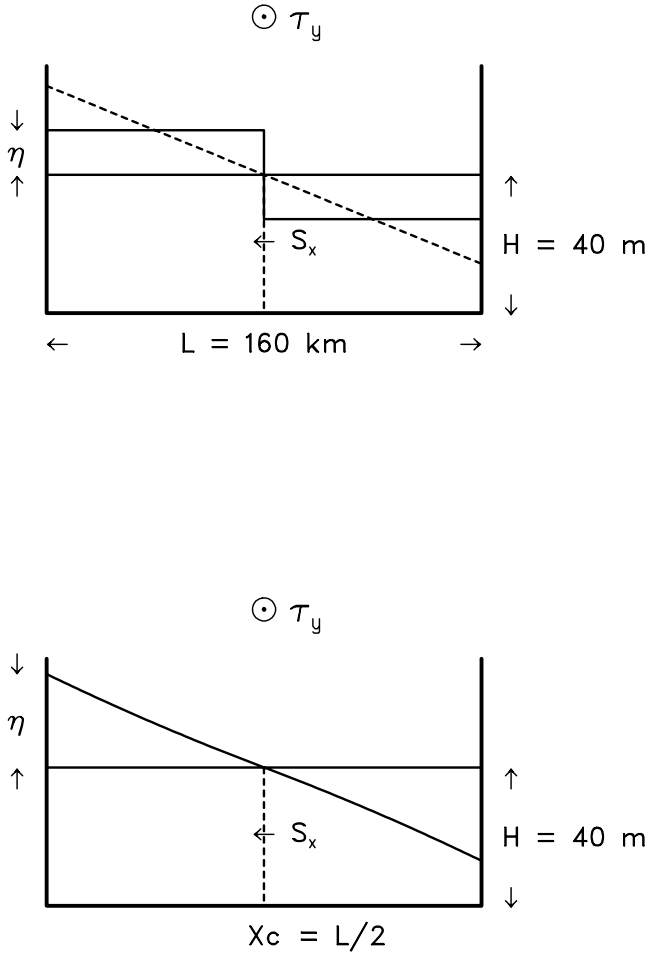


Figure 4. Diagrams for an idealized Taiwan Strait cross-shore section where measurement is made for deriving the analytic solutions. The strait width at the location is about 160 km. A constant water depth of 40 m, approximation of the average depth, is used.

$$S_v = 8 (gH/f^2) (\tau_y/\rho) / L. \quad (3)$$

[16] The transport through a strait can also be derived by applying the solution for the linear, barotropic, coastally trapped Kelvin wave, a solution of continuity and geostrophy along a coast with constant water depth. The solution provides for the alongshore current (the cross-shore current is zero). In this case, the solution for the elevation, $\eta = A e^{-x/R} \cos(ky - \omega t)$, is applied. Adapting the solution to a strait (Figure 4),

$$\begin{aligned} \eta &= A \left(e^{-x/R} - e^{-X_c/R} \right) \cos(ky - \omega t) \text{ if } x \leq X_c, \\ &= -A \left(e^{-(L-x)/R} - e^{-X_c/R} \right) \cos(ky + \omega t) \text{ if } x > X_c, \end{aligned} \quad (4)$$

where R is the Rossby radius of deformation, $R = c/f$, and c is the wave speed, $c = \sqrt{gH}$. With a constant depth, X_c is located at center of strait, $X_c = L/2$, to satisfy continuity. The term, $\cos(ky - \omega t)$ or $\cos(ky + \omega t)$, where k is the wave number and ω is the angular frequency, describes the wave

alongshore structure related to the wave length, $1/k$, and its propagation in time, t . The amplitude, A , is the maximum amplitude of the surface elevation at the coast. Applying the solution to a strait, the water depth at X_c , $Ae^{-X_c/R}$, the mean sea level, is subtracted from the surface elevation. The amplitude can be derived applying continuity with instantaneous response. The solution for the elevation (depression) at $y = 0$ is

$$\begin{aligned} \eta &= -\frac{S_x}{R} \frac{e^{-x/R} - e^{-X_c/R}}{1 - e^{-X_c/R} - (X_c/R)e^{-X_c/R}} \text{ if } x \leq X_c, \\ &= +\frac{S_x}{R} \frac{e^{-(L-x)/R} - e^{-X_c/R}}{1 - e^{-X_c/R} - (X_c/R)e^{-X_c/R}} \text{ if } x > X_c, \end{aligned} \quad (5)$$

where S_x the cross-shore unit transport. Geostrophic current can be derived from surface slope, the gradient of cross-shore elevation. Integrating the current with depth across the strait and applying Ekman transport (equation (1)) for S_x , the transport through the strait can be directly related to the alongshore wind stress by

$$S_v = \frac{2 (gH/f^2) (\tau_y/\rho)}{R} \frac{1 - e^{-X_c/R}}{1 - e^{-X_c/R} - (X_c/R)e^{-X_c/R}}. \quad (6)$$

[17] If the half of the strait width, X_c , is small compared to the Rossby radius of deformation, exponential term of X_c/R can be expanded in series and $O^3(X_c/R)$ or higher order terms ignored, $\exp(X_c/R) \sim 1 - X_c/R + (X_c/R)^2/2$. Approximation may be made from equation (6),

$$S_v \sim 8 (gH/f^2) (\tau_y/\rho) / L, \quad (7)$$

which is exactly the same as equation (3).

[18] Applying the NOGAPS 3-hourly nowcast/forecast alongshore wind stress, the solutions of equation (6) and its approximation (equations (3) or (7)) are presented in Figure 5. The two solutions agree very well except at the peak of reversals when the currents are the strongest and the sea level becomes more exponential than linear. For the Taiwan Strait the Rossby radius of deformation is 280 km which is 4 times larger than the half strait width; therefore the approximation or equation (3) can be applied satisfactorily.

[19] The transport variation computed from the local numerical model forced by the wind stress at Taiwan Strait is compared to the analytical solution in Figure 6. Two solutions do not agree very well. The amplitude of reversals are larger for the analytical solution, particularly in the second event when the reversal is the strongest. The bottom friction, which the analytic solution does not consider, is the main source of the difference between two solutions. As shown in Figure 7, the amplitude of the reversals from the analytic solution is very close to the numerical solution without bottom friction. There are differences in the arrival time of the reversals between two solutions. The reversals from the analytic solution arrive earlier than the reversals from the numerical solution or the observations. The geostrophic current develops rapidly in response to the barotropic surface pressure forcing which acts on the whole water body. On the other hand, the Ekman transport, which is driven by the wind stress on the surface, needs time to

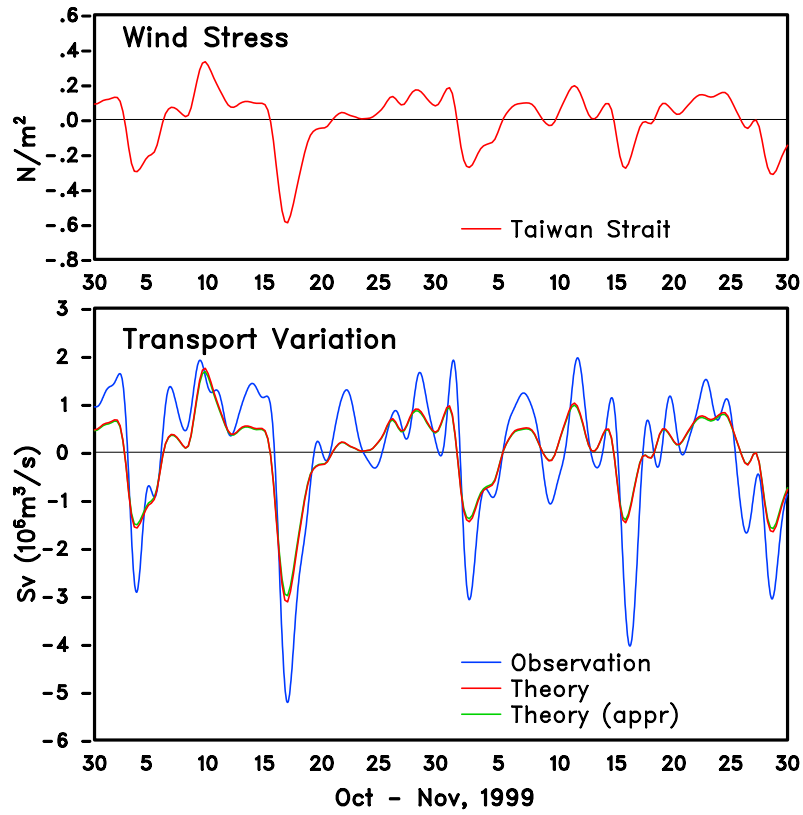


Figure 5. Transport variation time series from the analytic solution of equation (6) (red line) and from the approximation, equation (7) (green line), (top) forced by NOGAPS alongshore wind stress at Taiwan Strait. The observations (blue line) are superimposed.

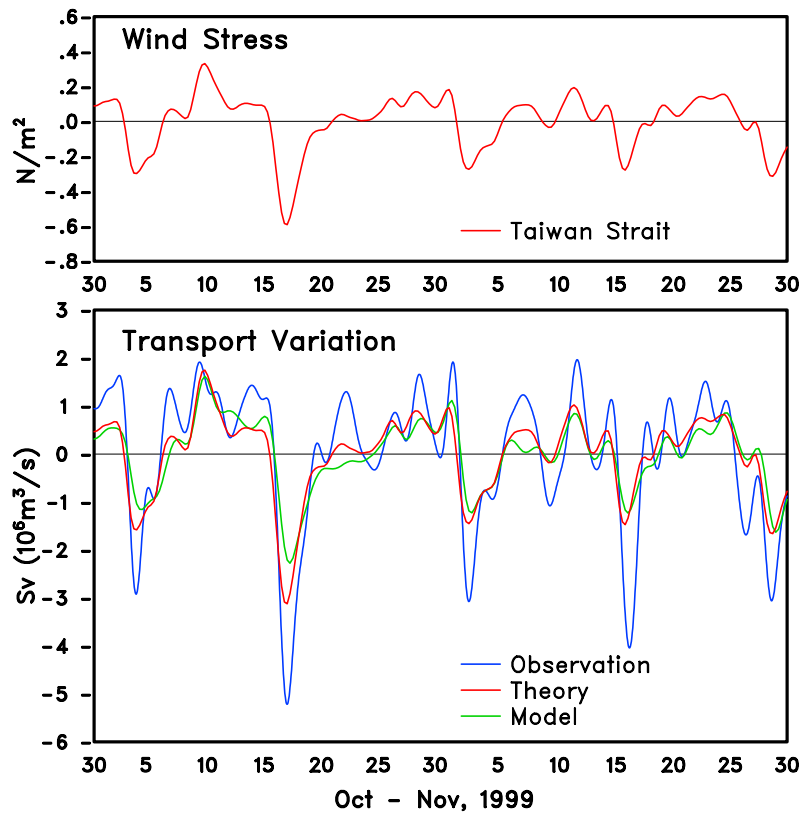


Figure 6. Transport variation time series from the numerical model (red line) and from the analytic solution (green line) forced by local wind compared to the observations (blue line).

fully develop as discussed by *Ekman* [1905]. The assumption of an instantaneous response of Ekman transport and the sea level setup to the wind stress is not accurate. In a study of Florida Current transport fluctuations caused by the local wind, *Lee and Williams* [1988] apply an analytical model adapted from *Csanady* [1982] to the Straits of Florida. In a comment regarding their work, *Chuang* [1988] suggests that since the ratio of the width to the barotropic Rossby radius of deformation in the Straits of Florida is very small ($L/R = 0.14$), Ekman transport may not develop. This is not the case in the Taiwan Strait where $L/R = 0.5$.

[20] The transport reversals induced by the local wind in both the analytical and numerical solutions are weaker than the observed reversals. Hence there must be other factors that contribute to the generation of these reversals.

4. Remote Wind Effect

[21] As suggested, the wintertime wind bursts in the Yellow Sea often excite coastally trapped waves, which propagate southward along the Chinese coast. Once the waves enter the Taiwan Strait, the cross-strait sea surface slope may reverse and induce a reversal of the transport through the strait. Examining the NPACNFS SSH during four observed transport reversals shows the coastally trapped waves in the Yellow Sea responding to strong northerly winds (Figures 8, 9, 10, and 11). The waves propagated from the Yellow Sea toward the South China Sea along the Chinese coast. In about 1.5 days, the waves entered Taiwan Strait. The arrival of the waves coincided with the observed transport reversals (Figure 12). The propagation speed of the waves estimated from the time-distance plot of alongshore SSH in Figure 12 is 14 m/s. This speed is that for long surface gravity waves along the Chinese coast in the Yellow Sea and the East China Sea with an average water depth of 20 m. The waves are barotropic, coastally trapped Kelvin waves.

[22] An analytic solution can be derived for the transport variation at a strait induced by a passing coastally trapped wave remotely forced by the wind. Applying the solution for linear, coastally trapped Kelvin waves to a coast as shown in Figure 13, the cross-shore elevation is

$$\eta = A \left(e^{-x/R} - e^{-X_c/R} \right) \cos(ky - \omega t). \quad (8)$$

Equation (8) corresponds to one side of equation (4), except that in equation (8), X_c is not located at the center of the strait. Instead, X_c is located at a distance from the coast where the amount of water setup at the onshore side equals the amount of water set-down at the offshore side up to the Rossby radius of deformation to satisfy continuity and $X_c = -\ln(1 - \exp(-1))/R$. The amplitude, A , can be computed, and the solution for the sea surface elevation at the maximum amplitude, $y = 0$, following the wave propagation, $t = 0$, is

$$\eta = -\frac{S_x}{R} \frac{e^{-x/R}}{1 - e^{-X_c/R} - (X_c/R)e^{-X_c/R}}. \quad (9)$$

Equation (9) is similar to equation (5) but applied to $0 \leq x \leq R$. The cross-shore unit transport, S_x , can be related to the alongshore wind stress by the Ekman transport (equation (1)).

[23] Once the coastally trapped wave propagates into a strait, the geostrophic current can be derived from the cross-shore gradient of the surface elevation (equation (9)). The transport through the strait is obtained by integrating the geostrophic current with depth across the strait,

$$S'_v(t + \delta t) = \frac{(gH'/ff') (\tau_y(t)/\rho)}{R} \frac{1 - e^{-L/R}}{1 - e^{-X_c/R} - (X_c/R)e^{-X_c/R}}, \quad (10)$$

where ' indicates the local parameters in the strait. The time delay, δt , is the time for the wave to propagate from a remote source to the strait. For a distance, r , $\delta t = r/c$ where c is the phase speed. Equation (10) connects the remote wind forcing, τ_y , to the transport variation, S'_v , via the coastally trapped waves. For a coastally trapped wave generated in the Yellow Sea, it takes about 1.5 days to travel to Taiwan Strait at a speed of 14 m/s.

[24] The solutions from equation (10) and from the numerical model forced with wind stress in the Yellow Sea (the analytic solution uses northerly wind) are shown in Figure 14. The transport reversals in the analytic solution agree very well with the transport reversals in the numerical solution. The lack of positive transport variations in the analytic solution is because the analytical solution (equation (10)) is only for the maximum amplitude at $y = 0$ following the wave propagation.

[25] Adding the transports generated by the local wind and those generated by the remote wind in the Yellow Sea from analytic solutions and from numerical solutions, the total transport variations are shown in Figure 15. The amplitude of the computed transport reversals is closer to the observations but not as large. The difference between the analytic/numerical solutions and the observations is the largest for the second event and is the smallest for the third event. Reviewing the NPACNFS SSH fields shows that the strong northerly winds propagate almost in phase with the coastally trapped waves. In the second transport reversal event, the wave was enhanced in the East China Sea by a strong alongshore northerly wind (Figure 9). During the third event, the wind in the East China Sea was mainly offshore, and the wave was not enforced (Figure 10). As shown in Figure 16, the transport variation at Taiwan Strait increases when the wind forcing in the East China Sea is included in the numerical solution. The reversal in the second event becomes much stronger, but it has a smaller change for the third event compared to the solution forced with wind in the Yellow Sea. This is consistent with what is shown in the NPACNFS SSH predictions.

[26] The sum of transport variations from the numerical solution forced with wind in the Yellow Sea/East China Sea and with wind at Taiwan Strait is presented in Figure 17 together with the transport variation forced with wind over the entire model domain. These solutions explain all of the

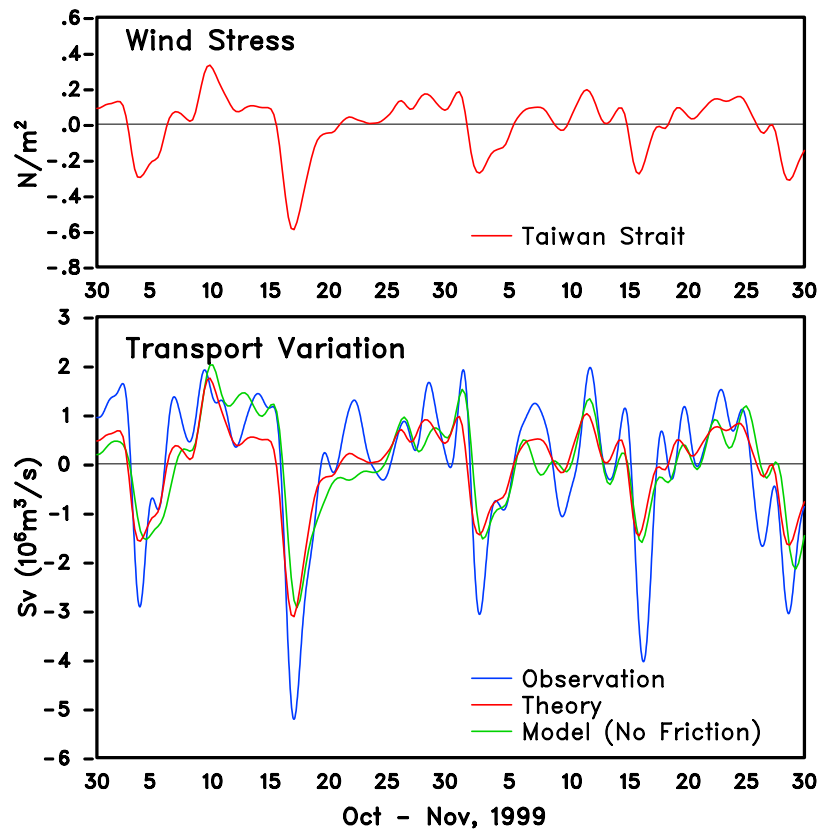


Figure 7. Transport variation time series from the numerical model without bottom friction (red line) compared to the analytic solution (green line). The observations (blue line) are superimposed.

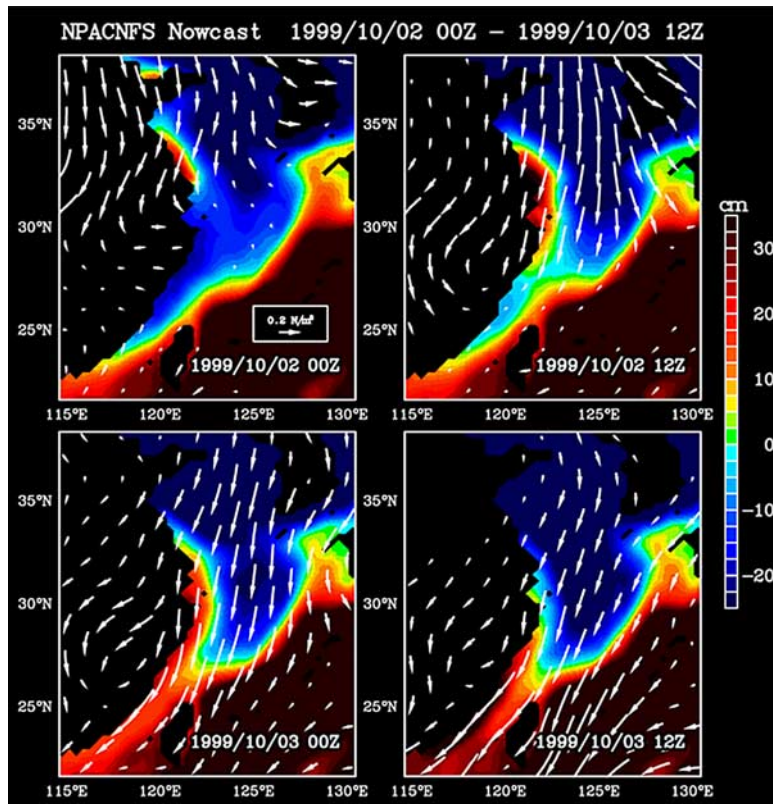


Figure 8. NPACNFS 12-hourly SSH predictions in the Yellow Sea, the East China Sea, and Taiwan Strait during the first transport reversal event from 2 October 1999 0000 UT to 3 October 1999 1200 UT. The NOGAPS wind stress vectors are superimposed.

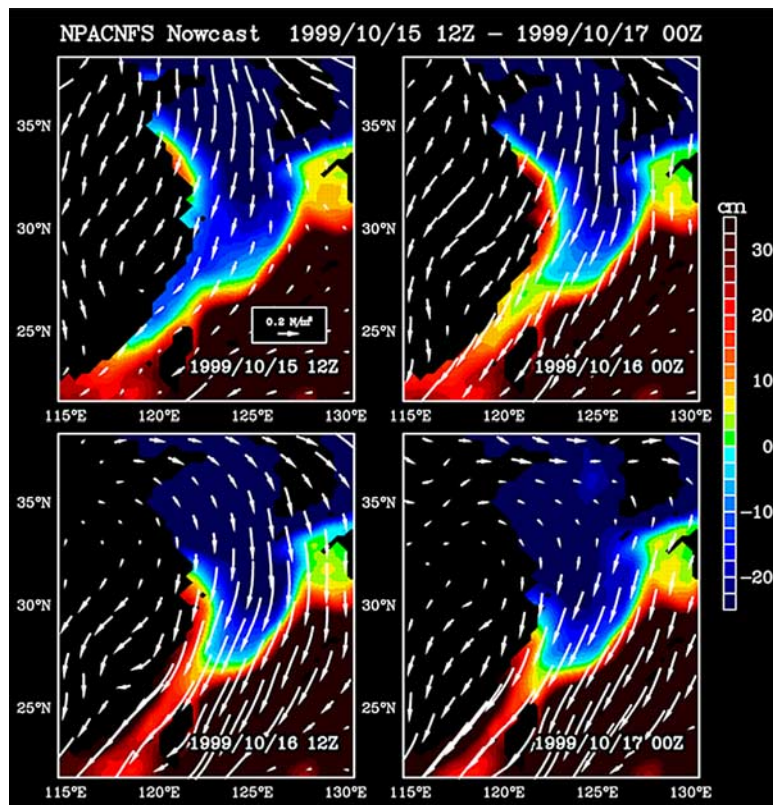


Figure 9. NPACNFS 12-hourly SSH predictions during the second transport reversal event from 15 October 1999 1200 UT to 17 October 1999 0000 UT.

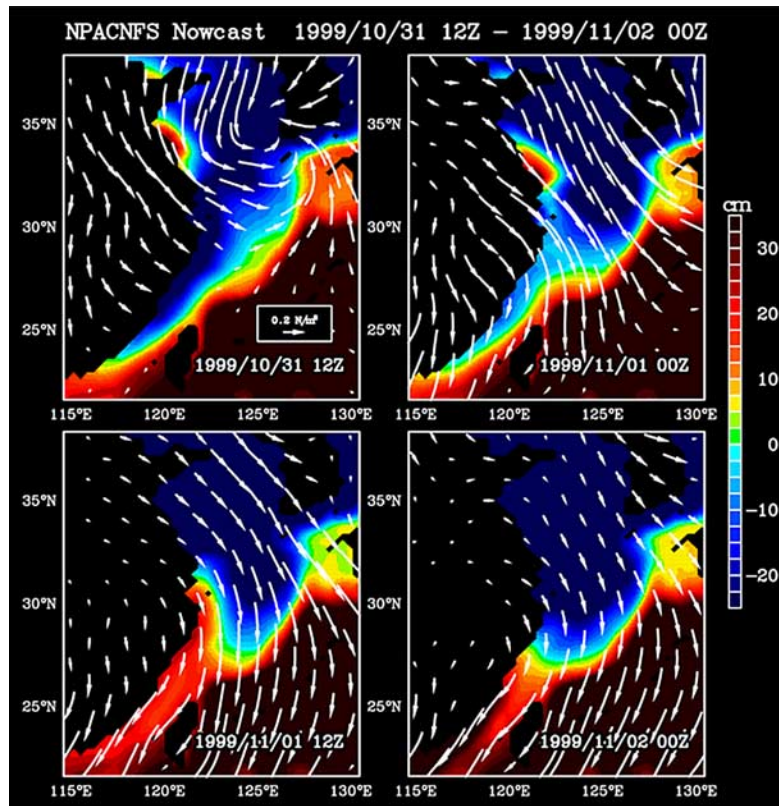


Figure 10. NPACNFS 12-hourly SSH predictions during the third transport reversal event from 31 October 1999 1200 UT to 2 November 1999 0000 UT.

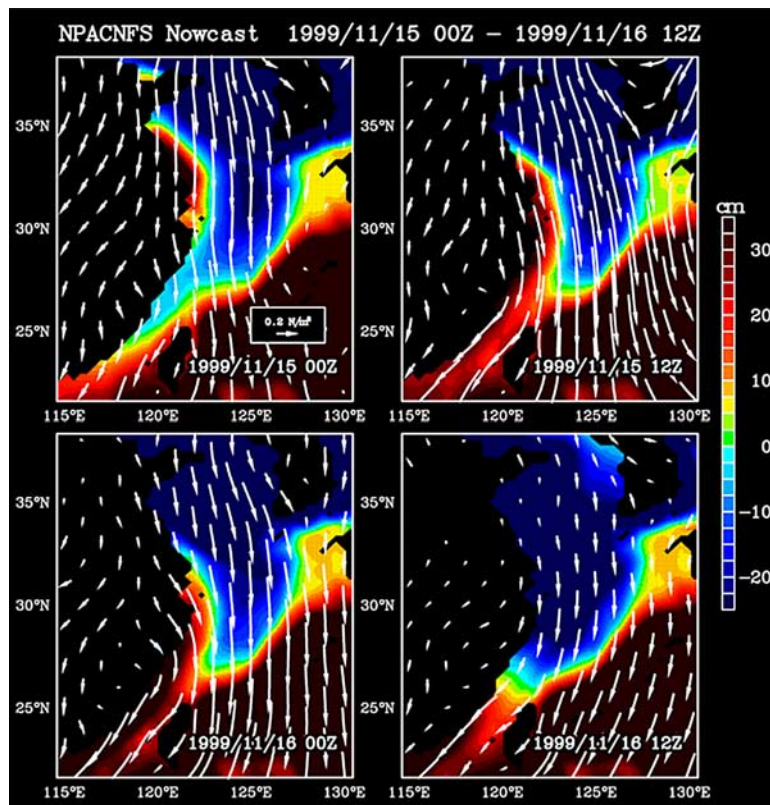


Figure 11. NPACNFS 12-hourly SSH predictions during the fourth transport reversal event from 15 November 1999 0000 UT to 16 November 1999 1200 UT.

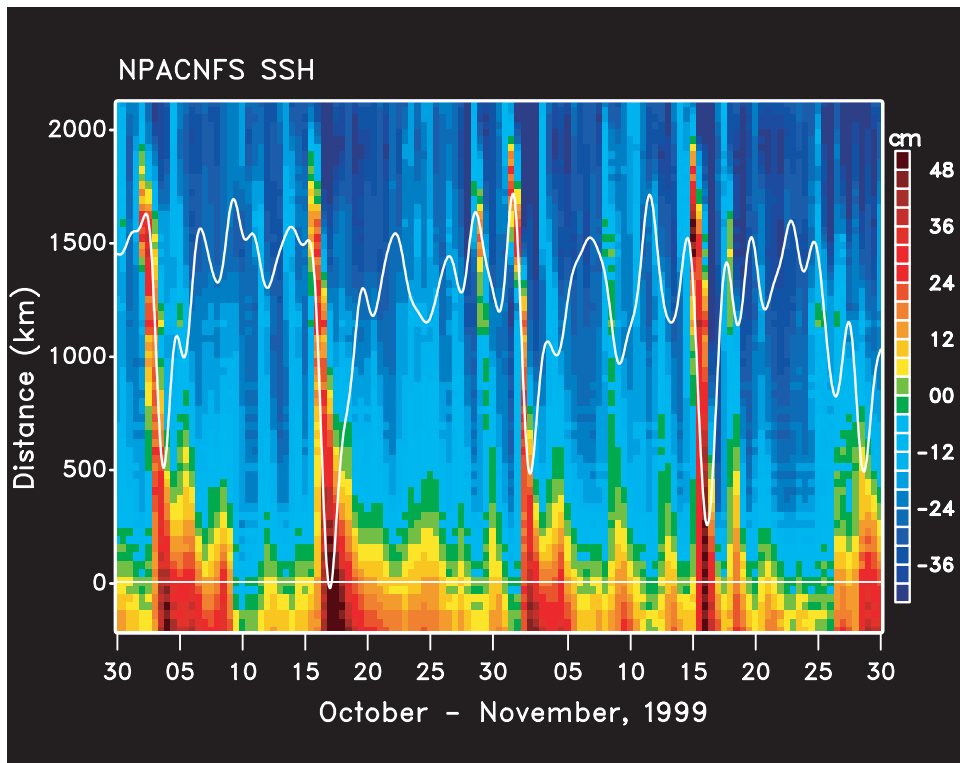


Figure 12. Time-distance plot of the alongshore NPACNFS SSH. The distance is from Taiwan Strait toward the Yellow Sea along the Chinese coast. The coastally trapped waves started in the Yellow Sea, propagated southward along the coast. The arrivals of the waves at Taiwan Strait coincided with the observed transport reversals (white line).

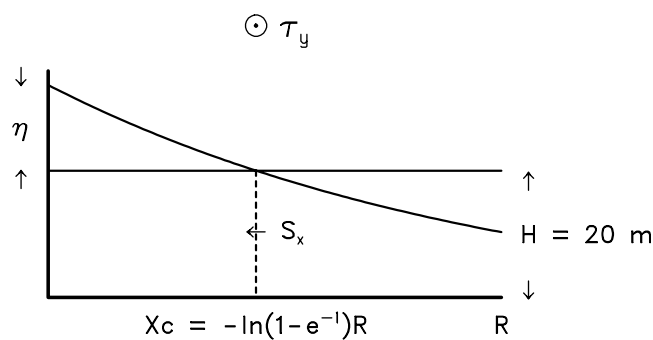


Figure 13. Diagram of an idealized Yellow Sea cross-shore section with coastally trapped wave. The water depth is taken to be 20 m. The latitude is 34°N and the Rossby radius of deformation, R , is 180 km.

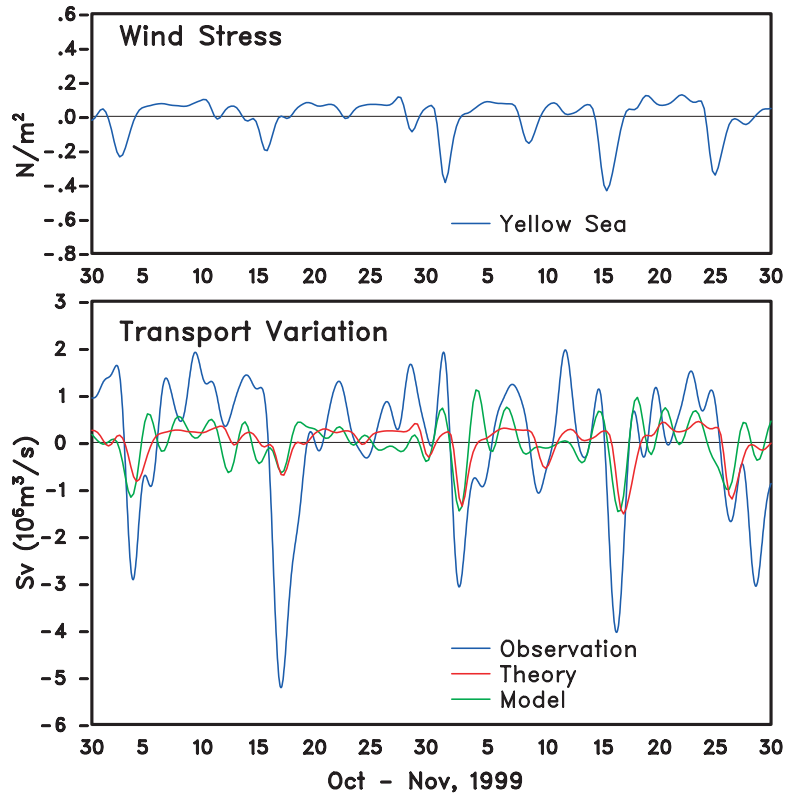


Figure 14. Transport variation time series from the analytic solution (red line) and from the numerical model (green line) (top) forced by remote wind in the Yellow Sea. The observations (blue line) are superimposed.

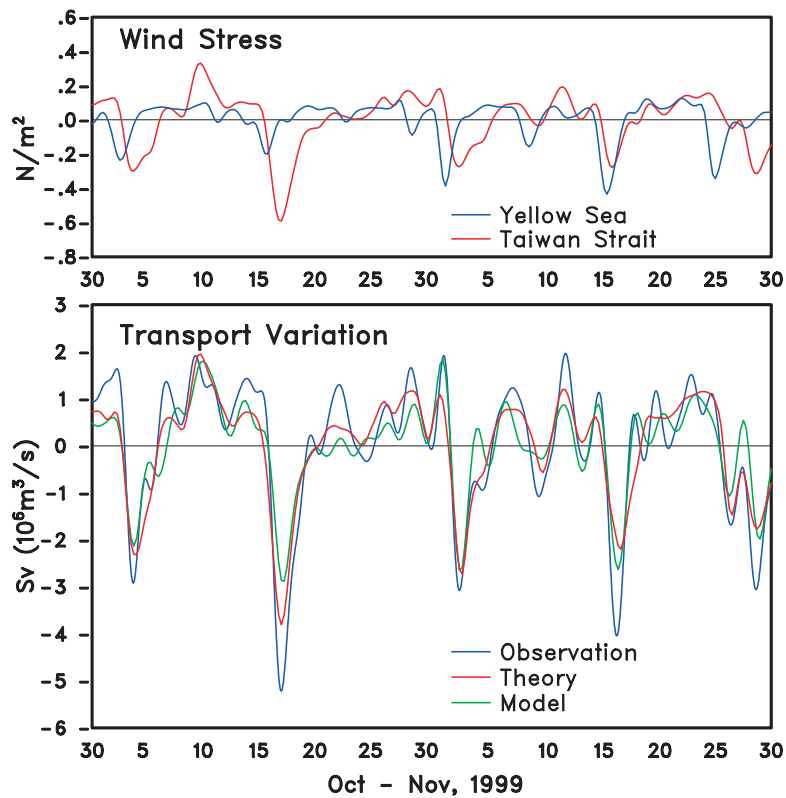


Figure 15. Sum of the transport variations computed with the remote wind in the Yellow Sea and with the local wind in Taiwan Strait from the analytic solution (red line) and from the numerical model (green line). The observations (blue line) are superimposed.

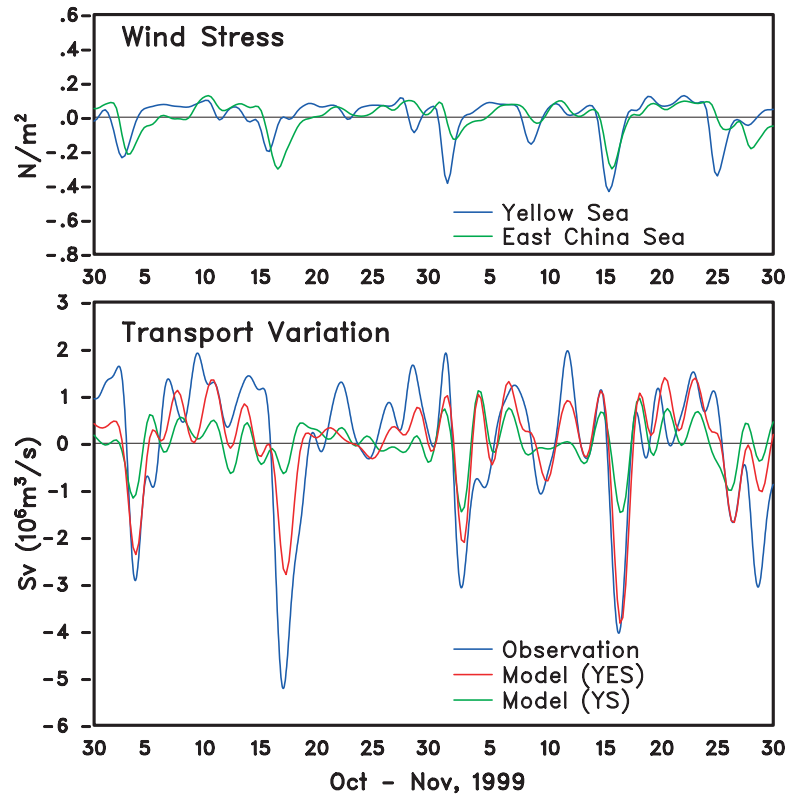


Figure 16. Transport variations time series from the numerical model forced by the remote winds in the Yellow Sea and East China Sea (red line) compared to the one forced by the remote wind in the Yellow Sea (green line). The observations (blue line) are superimposed.

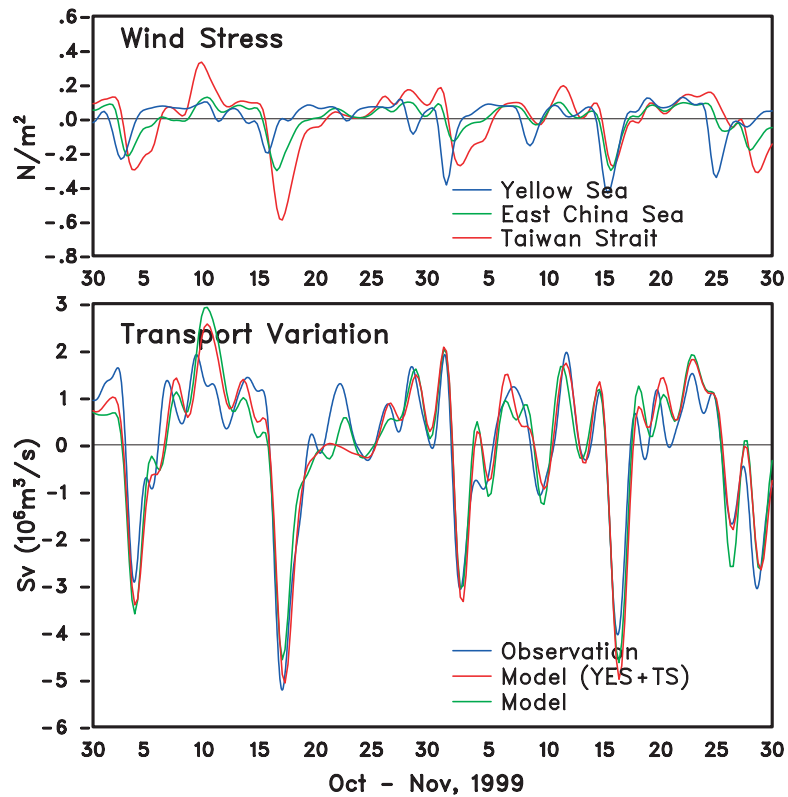


Figure 17. Time series for the sum of transport variations from the numerical model forced by the remote winds in the Yellow Sea and East China Sea and forced by the local wind in Taiwan Strait (red line). The transport variation from the numerical model driven with wind over the entire model domain is shown (green line). The observations (blue line) are superimposed.

four observed transport reversals at Taiwan Strait during the period of time.

5. Conclusions

[27] The strong periodic transport reversals observed in Taiwan Strait during October and November 1999 may be explained by a combination of local wind effects and coastally trapped waves remotely generated in the Yellow Sea by the wintertime wind bursts. The coastally trapped waves propagate southward along the Chinese coast and are enhanced by the alongshore wind in the East China Sea.

[28] **Acknowledgments.** This work was sponsored by the Office of Naval Research as part of the “Relocatable Model Development and Evaluation” (PE0602435N) and as part of the “Dynamical Linkage of the Asian Marginal Seas” (PE0601153N) projects. This work is a contribution of the Naval Research Laboratory, JA/7320-02-3. We are grateful to Paul Martin for helpful review of this manuscript.

References

- Blumberg, A., and G. Mellor, A description of a three-dimensional coastal ocean circulation model, in *Three-Dimensional Coastal Ocean Models, Coastal Estuarine Sci.*, vol. 4, edited by N. Heaps, pp. 1–16, AGU, Washington, D. C., 1987.
- Carnes, M. R., D. N. Fox, R. C. Rhodes, and O. M. Smedstad, Data assimilation in a North Pacific Ocean monitoring and prediction system, in *Modern Approaches to Data Assimilation in Ocean Modeling, Oceanogr. Ser.*, vol. 61, edited by P. Malanotte-Rizzoli, pp. 319–345, Elsevier Sci., New York, 1996.
- Chern, C.-S., A preliminary study on the response of Taiwan Strait to winter monsoon, *Acta Oceanogr. Taiwan.*, 13, 124–139, 1982.
- Chuang, W.-S., Dynamics of subtidal flow in the Taiwan Strait, *J. Oceanogr. Soc. Jpn.*, 41, 65–72, 1985.
- Chuang, W.-S., A note on the driving mechanisms of current in the Taiwan Strait, *J. Oceanogr. Soc. Jpn.*, 42, 355–361, 1986.
- Chuang, W. S., Comments on “Wind-Forced Transport Fluctuations of the Florida Current,” 18, 1755–1756, 1988.
- Csanady, G. T., *Circulation in the Coastal Ocean*, 279 pp., D. Reidel, Norwell, Mass., 1982.
- Ekman, V. W., On the influence of the Earth’s radiation on the ocean current, *Ark. Math. Astron. Fysik.*, 2(11), 1–53, 1905.
- Hsueh, Y., Recent current observation in the eastern Yellow Sea, *J. Geophys. Res.*, 93, 6875–6884, 1988.
- Hsueh, Y., and I. C. Pang, Coastally trapped long waves in the Yellow Sea, *J. Phys. Oceanogr.*, 19, 612–625, 1989.
- Hu, D. X., Some striking features of circulation in the Huanghai Sea and East China Sea, *Oceanol. China Seas*, 1, 27–38, 1944.
- Jacobs, G. A., R. H. Preller, S. K. Riedlinger, and W. J. Teague, Coastal wave generation in the Bohai Bay and propagation along the Chinese coast, *Geophys. Res. Lett.*, 25(6), 1998a.
- Jacobs, G. A., W. J. Teague, S. K. Riedlinger, R. H. Preller, and J. P. Blaha, Sea surface height variations in the Yellow and East China Sea: 2. SSH variability in the weekly and semiweekly bands, *J. Geophys. Res.*, 103, 18,479–18,496, 1998b.
- Lee, T. N., and E. Williams, Wind-forced transport fluctuations of the Florida Current, *J. Phys. Oceanogr.*, 18, 937–946, 1988.
- Mellor, G. L., and T. Yamada, Development of a turbulence closure model for geophysical fluid problems, *Rev. Geophys.*, 20, 851–879, 1982.
- Rosmond, T. E., The design and testing of the Navy Operational Global Atmospheric Prediction System, *Weather Forecast.*, 72(2), 262–272, 1992.

G. A. Jacobs, D. S. Ko, and R. H. Preller, Naval Research Laboratory, Stennis Space Center, Code 7320, MS 39529, USA. (jacobs@nrlssc.navy.mil; ko@nrlssc.navy.mil; preller@nrlssc.navy.mil)

S. F. Lin and T. Y. Tang, Institute of Oceanography, National Taiwan University, Taipei, Taiwan. (linsf@itri.org.tw; tyt@ccms.ntu.edu.tw)